T-ASE-2016-258

Indirect Temperature Measurement and Control Method for Cell Culture Devices

Antti-Juhana Mäki, Tomi Ryynänen, Jarmo Verho, Joose Kreutzer, Jukka Lekkala, and Pasi Kallio,
Member, IEEE

***Abstract*—Microfluidic devices are promising tools with which to create an environment that mimics a cell's natural microenvironment more closely than traditional macroscopic cell culture approaches. In these devices, temperature is one of the most important environmental factors to monitor and control. However, direct temperature measurement at the cell area can disturb cell growth and potentially prevent optical monitoring, and is typically difficult to implement. On the other hand, indirect measurement could overcome these challenges. Therefore, using system identification method, we have developed models to estimate the cell area temperature from external measurements without interfering cells. In order to validate the proposed models, we performed large sets of experiments. The results show that the models are able to catch the dynamics of temperature in a desired area with a high level of accuracy, which means that indirect temperature measurement using the model can be implemented in future cell culture studies. The usefulness of the model is also demonstrated by simulations that use estimated temperature as a feedback signal in a closed-loop system. We also present tuning of a model-based controller and a noise study, which shows that the tuned controller is robust for typical ambient room temperature variations.**

Note to Practitioners:
In this paper, we tackle the problem related to temperature measurement in microfluidic devices, especially but not only concerning cell culture environments. Even though it would be desirable to place a temperature sensor as close as possible to the location of interest, practical limits usually prevent this; for instance, limited space and requirements for optical monitoring. To overcome these problems in microfluidic devices, we present a novel indirect temperature measurement approach using system identification method. Idea is to create a model that estimates temperature on the area of interest using measured outside temperature. Because it is required to measure both model input and output signals for the model development, we first fabricated a temperature sensor plate, combined it with our heating system, and measured required temperatures on several experiments. Then, we developed third-order discrete state-space models using measured temperatures and System Identification Toolbox in MATLAB. Model performances were examined and compared to measurements. Furthermore, we created a closed-loop Simulink (from MATLAB) model, and showed how desired temperature could be controlled using only measured outside temperature and the developed model. In future research, we will implement the designed closed-loop system to our cell culture system to precisely control temperature in the cell area.

***Index Terms*—Control, microfluidics, numerical simulation, system identification, thermal analysis**

I. Introduction

Using microfluidic devices as a research tool for biological cell studies is attractive because of such devices have lower costs, significantly faster reaction times, and lower power and reagent consumption than conventional methods [1]. In such studies, it is crucial to properly maintain and control physiological environmental factors such as oxygen, pH, and temperature in order to support cell growth and proliferation. Microfluidic devices provide substantial benefits compared to macroscopic cell culturing solutions because they offer the possibility for more precise control of these environmental factors. In brief, their ability to mimic a cell's natural microenvironment is significantly better, which means that more realistic responses from the cultured cells can be expected. [2]-[4] The fact that these devices use much smaller volumes than conventional systems such as cell culturing in flasks makes it possible to achieve better control of environmental parameters. [5] For example, temperature control of the microenvironment of cells in microscopic devices can be much more precise, requires considerably less power, and can still provide device performance that is several times

Manuscript received April 8, 2016; revised July 8, 2016 and September 15, 2016; accepted September 20, 2016. This work was supported by Doctoral Programme of the President of the Tampere University of Technology (TUT) and Tekes, the Finnish Funding Agency for Technology and Innovation (Decision no. 40332/14). The work was carried out within the Human Spare Parts 2 project.

A.-J. Mäki, T. Ryynänen, J. Verho, J- Kreutzer, J. Lekkala, and P. Kallio are with the Department of Automation Science and Engineering, Tampere University of Technology, Korkeakoulunkatu 3, 33720 Tampere, Finland, and also with the BioMediTech, Institute of Biosciences and Medical Technology, Biokatu 10, 33520 Tampere, Finland (e-mail: antti-juhana.maki@tut.fi; tomi.ryynanen@tut.fi; jarmo.verho@tut.fi; joose.kreutzer@tut.fi; jukka.lekkala@tut.fi; pasi.kallio@tut.fi).

faster than macroscopic systems. Furthermore, using microsensors based on micromachining processes achieves much smaller, lighter, and easier installation and less power-consuming temperature measurements. [6]

An accurate measurement from a cell area is desirable for maintaining a physiological temperature for the cells, typically at 37°C. However, measuring temperature directly from the cell area has several drawbacks. The measurement can (negatively) affect cells and might prevent optical monitoring. Another disadvantage is that a larger cell culture chamber is needed to implement the temperature sensor inside the chamber close to cells [7]. Furthermore, in many cases it is significantly more difficult to place sensors in the region of interest than, for example, outside the cell culture chamber. Therefore, a non-destructive indirect temperature measurement is preferable compared to direct measurement from the cell area. For this reason, in many studies temperature sensors have been placed outside the cell area; for example, next to the cell culture device [8], together with the heating element [9]-[11], in the upstream and downstream of the center of the culture chamber [12], in the reference chamber [13]-[15] or on the tubing surface close to the inlet of the chip [16]. However, the problem in these cases is that usually the exact temperature on the cell area cannot be guaranteed. For example, temperature differences up to 2-3°C between the measured temperature and the temperature on the culture area have been reported [8]. One approach used for providing a uniform temperature profile is to build a complex and large insulated device where a water bath surrounds the chamber. Unfortunately, this typically leads to a longer temperature settling time during the heating phase, for example approximately 60 minutes in [15], or a minimum time of 5 min to change temperature for one degree [17].

Fluorescent labels have been used for direct temperature measurement in microfluidic devices. This method based on fluorescence intensity ratio (FIR) requires for mixing fluorescent dyes with the working fluid. While the method typically works well with glass-based materials, it cannot be used with porous materials, such as poly(dimethylsiloxane) (PDMS), because adsorption of dye particles increases the measured fluorescence intensity, thus preventing accurate temperature measurements. Even though there are methods to overcome the adsorption problem, they still experience a decreased device performance [18]. Furthermore, error of this method is typically approximately 2.5°C at 37°C [19], which remains typically too large for cell culture studies. For example, it has been reported that the cardiomyocyte beating characteristics is altered in temperatures between 37-39°C [20].

To overcome the discussed limitations, we propose here a new method to estimate temperature in a cell culture device based on an indirect measurement signal. The idea is to estimate the temperature in the area of interest using the developed models and the temperature measured from a more suitable location. This would enable, for instance, that during cell experiments we place a temperature sensor in a suitable location outside the cell area. This prevents placing another sensor in the area where cells are located which can block optical monitoring, for example.

The method proposed in this paper is based on a system identification process. Briefly, the system identification process can be understood as a modeling process in which the model is selected on the basis of measured input and output data. The process contains three elements: data, the model, and the criteria by which the model is chosen. [21] The advantage of this approach is that the model can be identified without knowing the precise underlying physical phenomena, and can still achieve model predictions that fulfill precision requirements. [22] Therefore, we have created two system identification-based black-box models between a temperature measured outside of the device and the temperature in the cell area. These models estimate the desired temperature, and this estimated temperature in the cell area can be used as a feedback signal to a heating system to close the control loop. Simulations are provided to illustrate the closed-loop system behavior, demonstrating that the system is able to maintain temperature in the cell area using only indirect measurement data and the developed model.

The remainder of this paper is organized as follows. Section II describes details on the used experimental setup and methods. Developed models are shown in Section III. Experimental data and simulation results are presented in Section IV; the developed models are validated and their performances are compared, before closed-loop system simulations using these models are presented. Also in Section IV, a temperature controller is tuned and a noise study is performed using simulations. Conclusions and discussion of the future work are provided in Section V.

II. Experimental

This section describes the measurements required for developing and validating the identification-based temperature models. First, the experimental setup is presented, including design of a temperature measurement system and calibration of the sensors. The measurements and the models developed are also described.

A. Design and fabrication

The experimental setup was composed of three main components: (1) a heating system, (2) a temperature sensor plate, and (3) a house-made six-well PDMS chamber [23], referred to henceforth as a PDMS device. These components are shown in Fig. 1. As the heating system, we applied a commercial signal amplifier that is typically used for recording cell signaling on microelectrode array (MEA) plates. Instead of a MEA plate, we used a custom-made temperature sensor plate (TSP) to detect temperatures inside (*T_Ri*) and outside (*T_Ro*) the PDMS device, which is placed on the top of the TSP. The components are described in more detail below.

1) *Heating system*

An MEA1060-Inv amplifier system (Multi Channel Systems MCS GmbH, Germany), typically used for *in vitro* cell experiments to record electrophysiological signals and stimulate cells, was used as a platform for the temperature experiments. The heating system includes a heating element, a proportional-integral (PI) controller (Temperature Controller TC02), a temperature sensor (Pt-100, measures *T_heater* as shown in Fig. 1(b)), and contact pads for the sensor plates. It should be noted that since passive cooling is used, the ambient room temperature is always the minimum achievable

temperature. For microscopic inspection, there is a hole (8 mm in diameter) in the center of the heating element. In this study, we by-passed pre-amplifiers of MEA1060-Inv, and used it only for warming the device and to provide good and stable mechanical and electrical connections between measurement electronics and TSP. During experiments, we manually changed the set-point temperature of the heating element (marked as *T_set* in Fig. 1(b)). Furthermore, the maximum heating power for the heating element was always kept at the recommended 12 W. [24], [25]

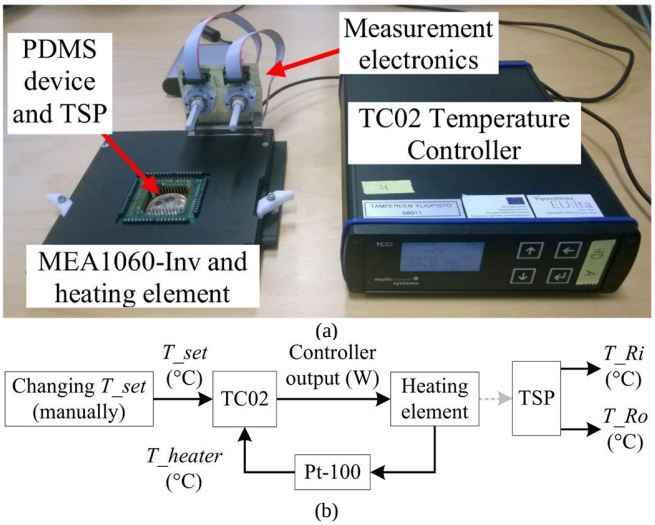

Fig. 1. Experimental setup: (a) a photograph of the whole system, and (b) a block diagram of the measurement process.

2) *Temperature sensor plate*

Fig. 2 shows the design of the TSP and the measurement electronics. A sensor layout including 14 resistors, each using a four-wire measurement, was implemented. In this paper, only two resistors fabricated from copper, marked as *Ri* and *Ro* in Fig. 2(a), are used for measuring *T_Ri* and *T_Ro*, respectively. The layout was designed so that it can be used together with connection pins in MEA1060-Inv. In TSP, both of the used resistors (*Ri* and *Ro*) have the following dimensions: a thickness of 275 nm, a line-width of 20 µm, a total length of approximately 25.7 mm, and a total area of approximately 0.51 mm^2. The width of the tracks from the sensors to the contact pads shown in Fig. 2(a) is 100 µm. The plate was fabricated as follows: first, a custom-sized (49 mm ´ 49 mm ´ 1 mm) microscope slide (Menzel GmbH, Germany) was cleaned with acetone, isopropanol, and oxygen plasma (Vision 320 Mk II RIE, Advanced Vacuum Scandinavia AB, Sweden) before applying NR9-3000PY photoresist (Futurrex, USA) and patterning it with µPG501 maskless exposure system (Heidelberg Instruments, Germany). 275 nm of copper was e-beam evaporated 5 Å/s with a Meissner trap equipped with an Orion Series BC-3000 e-beam coater (System Control Technologies, USA) followed by a lift-off with acetone in an ultrasonic bath. The metal thickness was verified by Dektak XT contact profilometer (Bruker, USA). Next, approximately 500 nm Si_3N_4 insulator layer was deposited using Plasmalab 80+ PECVD (Oxford Instruments, UK). PR1-2000A photoresist (Futurrex, USA) was used as an etching mask when the Si_3N_4 was removed above the contact pads. Finally, the copper contact pads were polished by gently wiping them with a piece of cleanroom wipe moistened with isopropanol. An image of the fabricated plate is shown in Fig. 3.

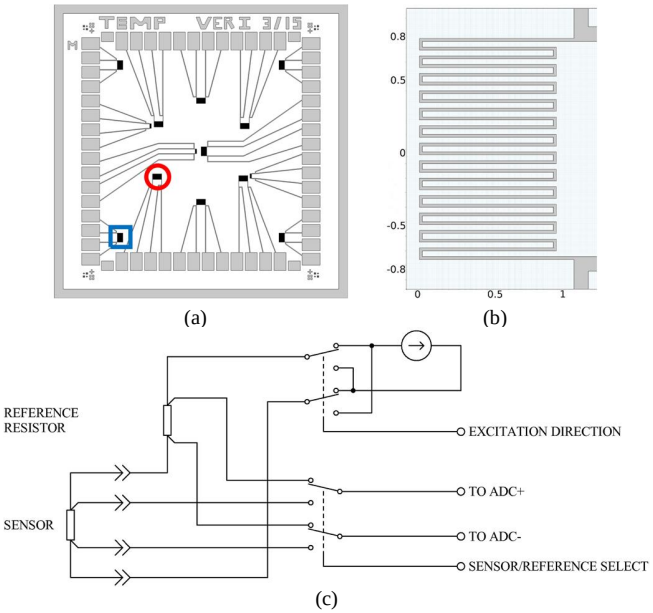

Fig. 2. Temperature sensor plate: (a) designed layout. Resistors used in this paper as temperature sensors are marked with a red circle (*Ri*) and a blue square (*Ro*). (b) A zoomed image of the used resistor (dimensions in mm), and (c) a schematic of a four-wire resistance measurement circuit.

In order to measure and log the resistances of the chosen sensors, a dual-channel four-wire resistance meter was built. In this measurement circuit, shown in Fig. 2(c), 0.59 mA constant current sources were used for sensor excitation, such that the power dissipation, and thus the heating of the actual sensing elements, were independent of the wiring resistances. However, instead of relying on the accuracy and stability of the current sources and the sensor voltage measurements, additional highly precise and stable reference resistors (PCF0805 series, TT electronics, USA) were connected in series with the sensor resistors and the current sources. A multiplexing arrangement was used to measure both the sensor resistor voltages and the reference resistor voltages using the same voltage measurement hardware. Thus, in this arrangement, the measured resistance was the ratio of the two voltages multiplied by the reference resistor's resistance. The actual voltage measurements were performed using a 24-bit A/D-converter (LTC2445, Linear Technology, USA). An additional switching arrangement was included to reverse the excitation current direction periodically so that synchronous detection could be used to remove the effects of offset voltages, noise pick-up by sensor wiring and other similar sources of error. The chosen 20.8 Hz excitation frequency was a compromise between noise rejection and ease of implementation. Next, the resistance results of 21 excitation frequency cycles were averaged, providing a measurement frequency of approximately 1 Hz. The raw measurement data were transmitted to a computer using a USB connection and stored for further processing. Initial measurements using 100Ω dummy sensors (RNC90Y series, Vishay, USA) showed 0.11

mΩ root-mean-square noise and 1.4 mΩ initial warm-up drift. Measured resistance values of the fabricated resistors were approximately 110 Ω at the room temperature. This resistance was larger than we expected based on our simulations (approximately 80 Ω) using typical electric properties of copper. Therefore, the resistivity of the fabricated copper layer was approximately 1.4 times larger than the typically reported bulk resistivity of copper (16.7 nΩ·m in [26]).

3) *PDMS device*

The PDMS device, shown in Fig. 3, was composed of two PDMS parts and a glass plate as a lid. PDMS was chosen because of its suitability for rapid prototyping, biocompatibility and optical transparency [27], [28]. The fabrication process of the similar six-well PDMS chamber was presented earlier [23]. Briefly, the device was fabricated from two PDMS parts by mixing PDMS prepolymer and curing agent (Sylgard 184, Dow Corning, USA) in a standard 10:1 ratio. The top part, which provided the walls of the containers, was punched from a bulk (thickness 6 mm) PDMS sheet using a 32 mm diameter custom-made punch. Thereafter, three 6 mm Ø holes and three 8 mm Ø holes, 8.45 mm distance from the middle of the disk, were punched through the disk for the medium reservoirs using custom-made punches. The bottom part was punched from a bulk (thickness 1 mm) PDMS sheet with the same 32 mm diameter punch. The two parts were bonded irreversibly using an oxygen plasma treatment (Vision 320 Mk II RIE, Advanced Vacuum Scandinavia AB, Sweden). The six openings for the cell cultivation areas (diameter: 3 mm) were punched through the membrane using a biopsy punch. After fabrication, the device was stored in a closed Petri dish at normal room temperature and humidity. The lid of the device, a 1-mm-thick glass plate (diameter: 32 mm), was pressed to reversibly close the system before experiments, resulting in the final PDMS device diameter and the total height being 32 mm and 8 mm, respectively.

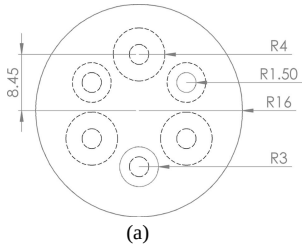

(a)

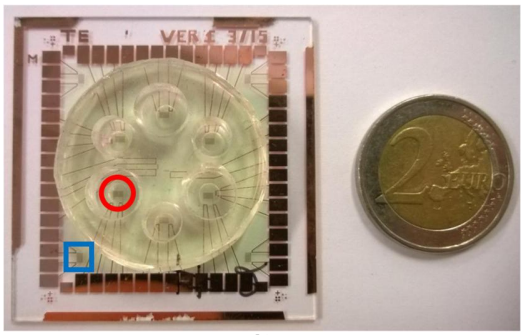

(b)

Fig. 3. (a) Schematic of the PDMS device and (b) an image of the fabricated PDMS device on the top of the TSP. Resistors used in the experiments are marked with a red circle (*Ri*) and a blue square (*Ro*).

B. Sensor calibration

Calibration of the chosen resistors was performed in a temperature-controlled oven (UN 55, Memmert GmbH, Germany). Six different temperature (*T*) points between room temperature (approximately 24°C) and 37°C were chosen. A calibrated digital thermometer (VWR 620-2000, VWR Internatiol, Belgium) was used as a reference measurement device and was placed close to the resistors. First, the temperature measurement plate was placed inside the oven. When the reference thermometer showed that the temperature was saturated, a 20-second-long resistance measurement was recorded and an average resistance (*R*) value in that temperature was calculated. When all the data points were gathered, a first-order line fitting was implemented using MATLAB (version R2015a, The MathWorks, Natick, Massachusetts, USA). A maximum difference smaller than 0.2°C and an average difference of 0.085°C between measured and fitted values were observed. Therefore, a linear calibration curve was verified to be accurate enough in the used temperature range and was used in the measurements to convert measured resistances to temperatures. The calibration results are shown in Fig. 4. The given equations are used to convert *Ri* and *Ro* to *T_Ri* and to *T_Ro*, respectively.

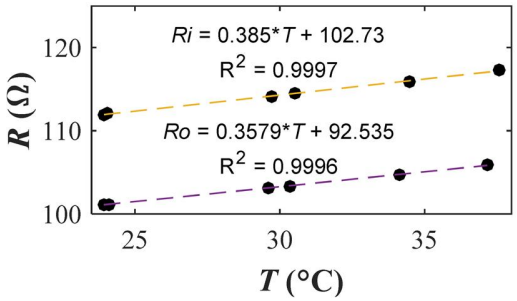

Fig. 4. Calibration curves for the selected resistors *Ri* and *Ro*: resistances as a function of temperature and their linear regression lines.

C. Measurements and developed models

In this paper, we designed three system identification-based models, as shown in Fig. 5. The first two models were developed for the indirect temperature measurement. The difference between these two models is the measured input signal that is used to estimate desired temperature. As our final goal is to implement this estimated temperature to a control-loop, and thus to be able to perform closed-loop simulations, we developed the third model. This model estimates temperature change of the heating element based on the controller output power.

We performed several measurements to estimate, validate, and test models that we had developed in this study. The entire experimental setup (see Fig. 1) was initially at room temperature and 200 µl de-ionized (DI) water was added to three 8 mm medium chambers in the PDMS device After approximately 30 s, a step change between 30°C and 40°C was manually set to the heating element using TC02. Unless otherwise stated, the recommended settings P = 6 W/K, and I = 0.9 W/(K·s) were used as the parameters of the PI temperature controller of the heating element [25].

Models 1 and 2 aim to estimate the temperature inside the PDMS device, *T_Ri*, based either on the measured heater

temperature *T_heater* or the temperature measured outside the PDMS device, *T_Ro*. Therefore, the input and output signals are *T_heater* and *T_Ri* for Model 1 and *T_Ro* and *T_Ri* for Model 2. Estimation and four validation measurements were performed to identify Model 1, while the same estimation measurement and two validation measurements were used to identify Model 2.

Model 3 estimates how much the PI controller's output power (W) heats the heating element, marked as *T_heat*. A sum of this and an ambient room temperature, *T_room*, provides *T_heater*, as shown in Fig. 5. By including Model 3 in closed-loop simulations, we were able to investigate, for example, how much *T_Ri* fluctuated when measured ambient room temperature variations were included in the simulation. Furthermore, implementation of Model 3 enabled us to improve the system performance; for instance, by accelerating the system response by PI controller tuning. Only a proportional controller (P = 1 W/K, I = 0 W/(K·s)) was used when collecting the estimation data for Model 3, and the default PI controller values were used in the validation measurement.

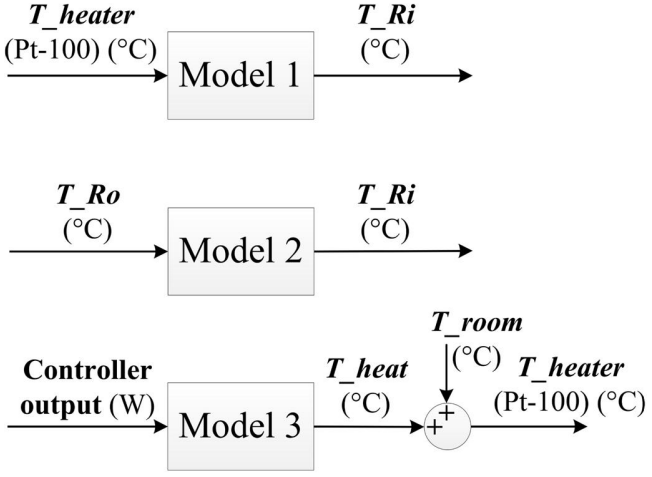

Fig. 5. Block diagrams of models.

To compare Models 1 and 2, an additional measurement was performed. The aim of this measurement was to mimic a temperature drop during visual inspection of cells, which is a routine step in cell culturing. During microscopic inspection, the TSP, together with the cells, needs to be placed from the heating system to a microscope and back after the inspection. This changes the temperature in the TSP and naturally the temperature of the cells. Therefore, we performed a test where the TSP and the PDMS device were moved from the room temperature to the pre-heated heating system. We also studied the sensitivity of Model 1 to changes in the liquid volume level in medium chambers

III. Developed Model Parameters

We used the System Identification Toolbox in MATLAB [29] to identify the models presented in Section II-C. Our objective was to estimate the system parameters using measured input and output data [30], and fit the model to the measured data regardless of the physical system; therefore, we used a black-box modeling technique. A prediction error method (PEM) was implemented to estimate the three models. This method selects models that make a prediction that is as close as possible to the true system if it was known. [21] The models were compared using a fit number, which is based on a Normalized Root Mean Square (NRMSE) criterion and can be calculated (as a percentage) using the following equation [29]:

$$fit = 100\left(1 - \frac{\|y - \hat{y}\|}{\|y - \bar{y}\|}\right) \quad (1)$$

where y, and $\hat{y}$ are the measured and estimated output, and $\bar{y}$ is the mean of y. Commonly used discrete-time state-space models include state variable vector $x(k)$, input variable vector $u(k)$, and output variable vector $y(k)$. The structure of the state-space models with three state variables used in this paper is as follows [29]:

$$\begin{aligned} x(k+1) &= Ax(k) + Bu(k) \\ y(k) &= Cx(k) + Du(k) \end{aligned} \quad (2)$$

where matrixes A, B, C, and D are state matrix, input-to-state matrix, state-to-output matrix, and feedthrough matrix, respectively. First, we tested second order state-space models and noticed that results compared to measured temperatures were not acceptable. Therefore, we chose third-order models as they provided good overall temperature estimation. Developed discrete-time models in this paper have the following form:

$$A = \begin{bmatrix} a11 & a12 & a13 \\ a21 & 0 & 0 \\ 0 & a32 & 0 \end{bmatrix}, B = \begin{bmatrix} b1 \\ 0 \\ 0 \end{bmatrix}, C^T = \begin{bmatrix} c1 \\ c2 \\ c3 \end{bmatrix}, D = d1 \quad (3)$$

The values of constants $a11$, $a12$, $a13$, $a21$, $a32$, $b1$, $c1$, $c2$, $c3$, and $d1$ in the three models are provided in Section IV-A. We estimated initial state values $x(0)$ from the first ten seconds of each measurement data using MATLAB.

IV. Simulation and Experimental Results

A. Validation of Models

Three different models were identified in this paper using the System Identification Toolbox, as described in Section III. Parameter values for the developed models are given in Table I. These state-space representations were used in simulations to compare the measured and modeled outputs. Each set of data was simulated in Simulink (The MathWorks, Inc., Natick, MA, USA) using the identified discrete state-space model with a sample time of one second.

TABLE I
MODEL PARAMETERS

Model #	*a11*	*a12*	*a13*	*a21*	*a32*	*b1*	*c1*	*c2*	*c3*	*d1*
Model 1	1.99	-0.99	0.00	1	1	2.0	0.29	-0.58	0.29	0.00
Model 2	1.99	-0.99	0.00	1	1	2.0	0.37	-0.74	0.37	0.00
Model 3	2.97	-1.47	0.48	2	1	0.5	0.15	-0.15	0.08	0.04

Model 1 was developed and validated with measurements shown in Fig. 6(a). The first measurement was used as the model estimation data, whereas four other measurements were used to study how well the model performed with different heating signals. For Model 2, we used three same experiments as for Model 1; the same estimation measurement and the first two validation measurements. The difference was that for Model 2 the measured *T_Ro* was used for the model input, as

shown in Fig. 5. Measured and simulated *T_Ri* are compared in Fig. 6(b). Analysis of the results is provided in the next section.

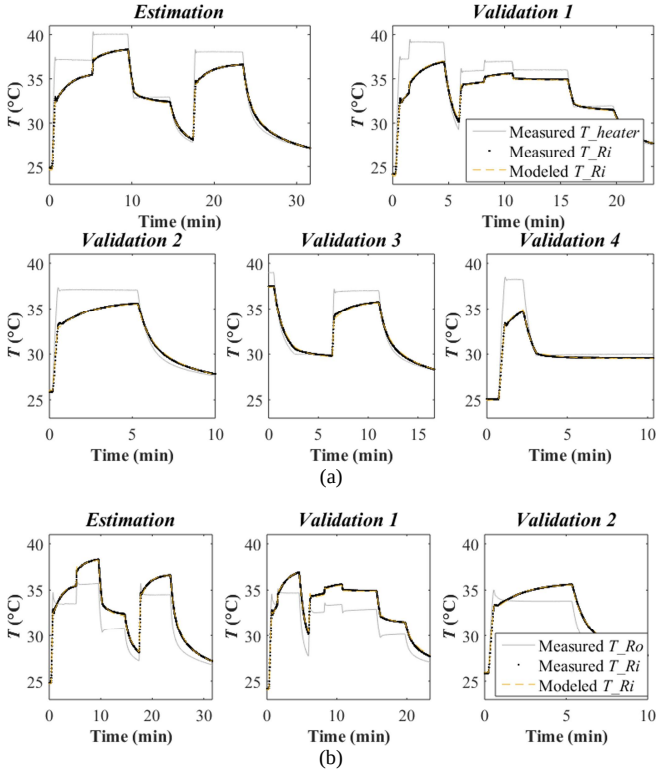

Fig. 6. Measurement and modeled data from (a) Model 1, where the input signal is *T_heater*, and (b) Model 2, where *T_Ro* is used as an input signal.

Model 3 was identified with two measurements, as reported in Section II-C. In the estimation measurement, a proportional controller (P = 1 W/K) was used because the input signal required for Model 3 was easier to obtain when using a P-controller (error signal is simply multiplied by value of P), thus enabling a simpler identification process. In both measurements, *T_set* was first set to 37°C and, after a while (approximately five to 15 minutes), heating was switched off and the system was passively cooled down. The resulting responses of the discrete state-space model compared to the measurement data are shown in Fig. 7.

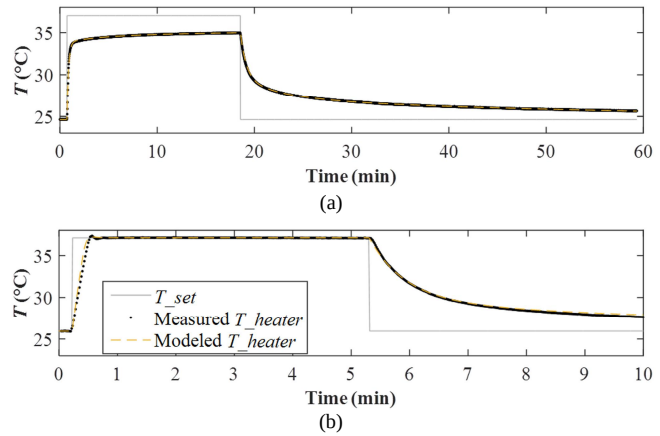

Fig. 7. Experimental and Model 3 comparison: (a) an experiment with only proportional control P = 1 W/K, and (b) an experiment with default PI controller values P = 6 W/K, and I = 0.9 W/(K·s).

As shown in Fig. 7(a), the error between the measured heater temperature and Model 3 output was negligible when proportional control was used. On the other hand, when the PI controller was implemented, Model 3 slightly overestimated the heating phase; modeled and measured rise times (time between 10% and 90% of the rise) were approximately 11 seconds and 14 seconds, respectively. However, this difference was still relatively low and insignificant compared to the response in the experiment overall, which means that the model could be used. In conclusion, based on the results reported in this section, it is clear that each of the developed models was able to estimate desired temperatures and could be used in closed-loop system simulations.

B. Performance analysis of Model 1 and Model 2

As Model 1 and Model 2 estimate *T_Ri*, their performance was compared. For this, two validation measurements presented in the previous section were used. The models were compared by calculating fit% (1), and average and maximum temperature differences between measured and modeled *T_Ri*, ΔT_{avg} and ΔT_{max}, respectively. The results are presented in Table II and in Fig. 8.

TABLE II
COMPARISON OF MODEL 1 AND MODEL 2 TO EXPERIMENTAL DATA

Model	**Model 1**		**Model 2**	
Measurement	*Validation 1*	*Validation 2*	*Validation 1*	*Validation 2*
Fit (%)	96.2	96.7	95.2	97.2
ΔT_{avg} (°C)	0.08	0.07	0.10	0.06
ΔT_{max} (°C)	0.52	0.44	0.69	0.27

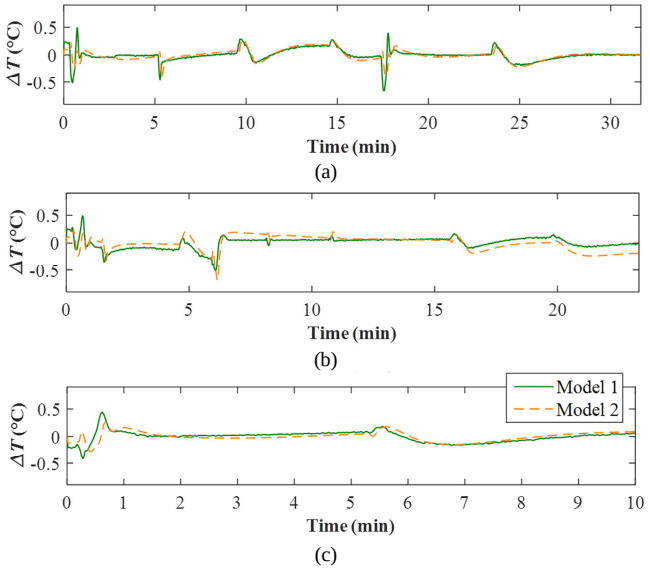

Fig. 8. Difference between measured and simulated temperatures when experiment is (a) *Estimation*, (b) *Validation 1*, and (c) *Validation 2*.

Based on the performance analysis, Model 1 performs slightly better. Therefore, it was chosen for closed-loop simulations in Section IV-D. However, Model 2 provides clear benefits in some cases, for instance, when a cooled TSP is placed on a pre-heated heating system. This is the case while moving the TSP from the heater to a microscope and back, a routine procedure performed during cell culturing. Fig. 9 shows the results of a study, where the device (at ~26.3°C) was placed on the heating

system (pre-heated to 37°C) at time 30 seconds, and temperature *T_Ri* was recorded and estimated using the two models.

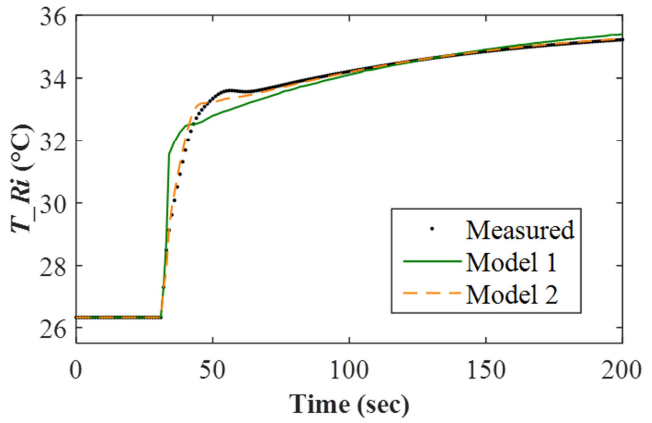

Fig. 9. Measured and simulated *T_Ri* when cooled temperature plate is brought to pre-heated heater.

In the pre-heated heater case, Model 2 estimated the output significantly more accurately than Model 1; fit% improved from 87.8% with Model 1 to 96.4% using Model 2. The reason was that now the heater and the TSP were initially in totally different temperatures, which meant that Model 1 overestimated *T_Ri* in the beginning of the measurement. To conclude, it is preferable to use Model 2 in cases where the heater and the TSP need to be separated during the study.

C. Sensitivity to liquid volume changes

Because the sensitivity of the model to environmental changes (disturbances) should be as small as possible, robustness of Model 1 to the volume in the system was studied next. The DI water volume in the three 8 mm chambers was changed ± 25% (from 200 µl to 250 µl or 150 µl). In Fig. 10 below, measurements with 250 µl and 150 µl volumes are compared to the model developed with 200 µl volume.

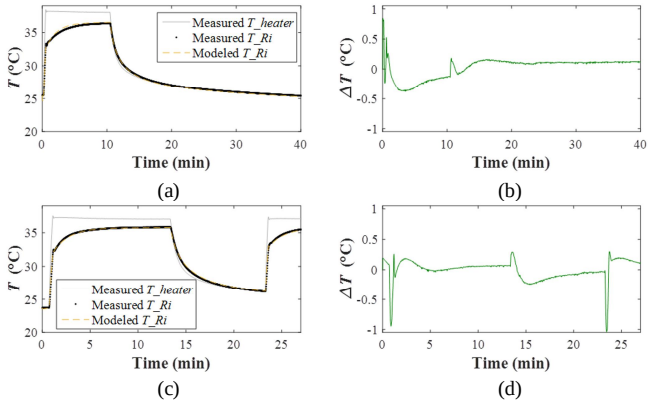

Fig. 10. Model 1 sensitivity tests for liquid volume change: (a) measurement and modeled data, (b) their difference when liquid volume is 250 µl, (c) measurement and modeled data and, (d) their difference when liquid volume is 150 µl.

As the results show, Model 1 was able to predict *T_Ri* well, which enables us to conclude that the model was not sensitive to volume changes. The difference between measurements and model predictions, ΔT_{avg} and ΔT_{max}, were now 0.14°C and 0.85°C for the liquid volume of 250 µl, and 0.11°C and 1.04°C for the liquid volume of 150 µl, respectively. It should be emphasized that reported ΔT_{max} last only very short period times, typically less than 10 seconds. One minute after the set point change, the errors are below 0.25°C in every measurement. Therefore, these results can be considered satisfactory in the planned applications, as a temperature variation of ± 0.3 to 1°C is generally still acceptable during cell cultivation [7], [14], [15], [17], [31]-[34]. As Model 1 was robust to volume changes, it is a useful temperature estimation tool in experiments with varying liquid volumes.

D. Closed-loop system simulations

The purpose of this section is to illustrate a method that can regulate *T_Ri* in the desired temperature using an indirect measurement signal. In this case, we would not need the inside sensor (*Ri*) at all. To demonstrate this approach, we present closed-loop simulations using the estimated temperature as a feedback signal by combining Models 1 and 3. First, to validate the performance of the developed closed-loop system, simulated *T_heater* was used as a feedback signal, as illustrated in Fig. 11(a). To regulate the temperature in the cell area, but not in the heater, we used *T_Ri* in the feedback loop, as shown in Fig. 11(b). Next, the performance of the default PI controller was analyzed and tuned, and a closed-loop system response with a tuned PI controller was then studied. Because of the limits of the real system (heating element power between 0 and 12 W [24]), saturation limits were also implemented in the PI controller in the model. For this reason, an integrator anti-windup design using clamping method [35] was implemented in the PI controller to stop integration when the output from the controller exceeds these saturation limits.

1) *Closed-loop system validation*

To validate the entire closed-loop system, shown in Fig. 11(a), Models 1 and 3 were implemented and simulated in Simulink. The same two measurements used for developing Model 3 (see Section IV-A) were also utilized here. The first measurement used proportional control (P = 1 W/K) and the second experiment was performed with the default PI controller (P = 6 W/K, and I = 0.9 W/(K·s)). Both the measurement and the simulation used *T_heater* as a feedback signal, as shown in Fig. 11(a). Modeled *T_heater* and *T_Ri* are in good agreement with the experimental data, as shown in Fig. 12; less than 0.5°C difference between the measured and modeled *T_Ri* was obtained from both experiments. This verified that a combination of Models 1 and 3 was able to estimate the desired temperature. With this control approach, the temperature in the cell area remains below the set point of 37°C.

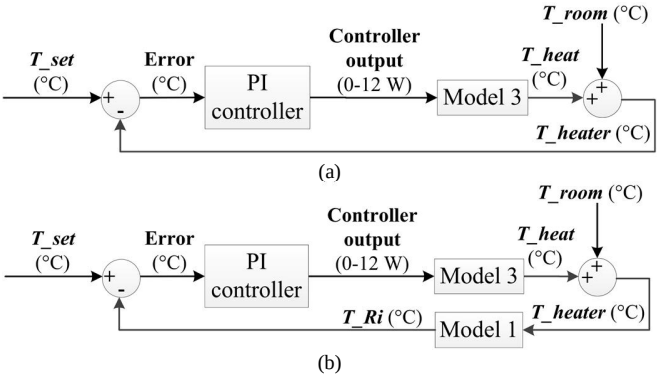

Fig. 11. Block diagram of a developed system when (a) *T_heater*, and (b) *T_Ri* is used as a feedback signal.

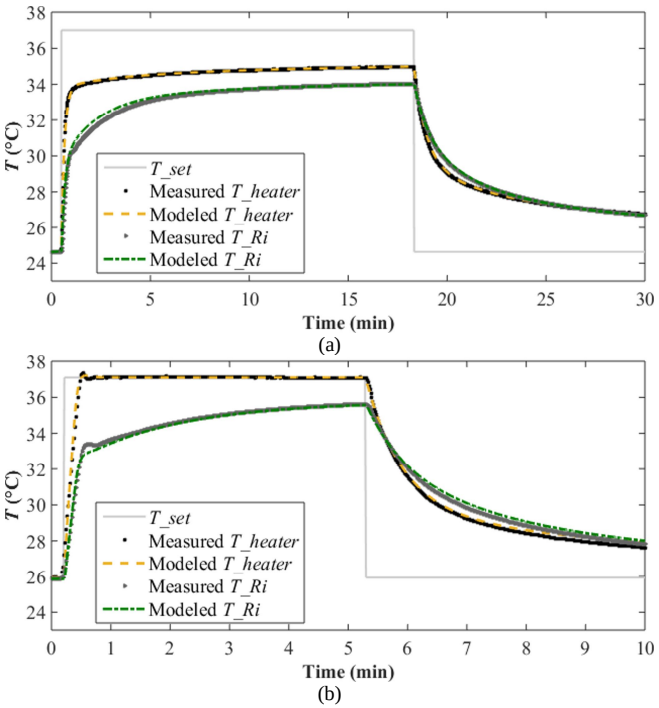

Fig. 12. Comparison of closed-loop system responses of measurement and simulation when (a) a proportional controller with P = 1 W/K, and (b) a PI controller (P = 6 W/K, and I = 0.9 W/(K·s)) was used.

2) *Controller tuning*

As stated, our goal is to develop a system that is able to control *T_Ri* using an indirect measurement signal and the developed models. Therefore, in contrast to the previous section, where we used *T_heater* as a feedback signal (Fig. 11 (a)), we first developed a model that used an output from Model 1 (*T_Ri*) as a feedback signal, as shown in Fig. 11 (b). We tuned the PI controller to improve the response of desired temperature *T_Ri*. The initial PI controller (P = 6 W/K, and I = 0.9 W/(K·s)) was simulated first and the controller parameters were then adjusted for a better performance. Our tuning goal was to decrease the overshoot and the settling time; therefore, we first increased the integral part. When an insignificant overshoot was achieved, we also increased the proportional part to accelerate the response until satisfying control results were achieved. A comparison of the system response with the default and the tuned PI (P = 9 W/K, and I = 1.2 W/(K·s)) controller is shown in Fig. 13.

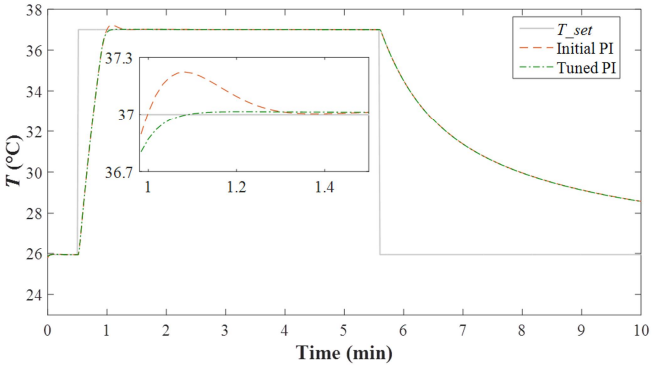

Fig. 13. Comparison of *T_Ri* with the initial (P = 6 W/K, and I = 0.9 W/(K·s)) and tuned (P = 9 W/K, and I = 1.2 W/(K·s)) controllers.

The comparison of the system responses with the default and tuned controller showed a small but improved response after tuning: overshoot was decreased from 0.22°C to a negligible 0.02°C with the same rise time of 21 seconds. The settling time (that is, the time it takes for the temperature to stay within ± 0.05°C of the set temperature 37°C) was decreased from 45 seconds to 32 seconds. To conclude, a better response with a smaller overshoot was achieved with the tuned controller.

3) *Noise study*

In the previous simulations, the ambient room temperature was approximated and was assumed to be constant. However, a more realistic situation should include temperature variations. For this reason, the developed model response with non-constant ambient room temperature was studied in this section. First, the ambient room temperature was recorded for 10 minutes, and the obtained signal was used as *T_room* value in the simulation. The measured ambient air temperature varied between 22.7°C and 22.9°C, as shown in Fig. 14.

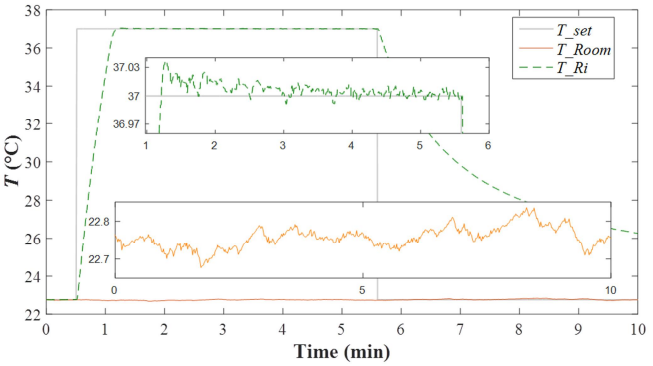

Fig. 14. Ambient air temperature variation study.

The ambient room temperature variation was included in the model and the system outcome was simulated. The results, presented in Fig. 14, showed that the controller was still able to keep *T_Ri* temperature at an acceptable level (± 0.03°C of the desired temperature of 37°C), which means that the controller is well suited for real applications where room temperature variations do exist.

V. Conclusion

This paper has presented a novel indirect temperature measurement method for microfluidic cell culture devices. The method is based on a system identification technique. The

developed mathematical models make it possible to indirectly measure and control temperature in desired locations. Therefore, this method can be used as a measurement and control tool in cell culture systems without interfering cultured cells. The proposed models were validated with several measurements and we have shown that estimated temperatures correlated well with experimental results. Results also demonstrated that the developed models were capable of catching the dynamics of the system temperature. Furthermore, the models were reasonably robust to environmental changes, such as remarkably large liquid volume changes, and measured ambient air temperature variations. Finally, the parameters of the controller used were tuned using simulations and a better system response was achieved. Our future work will include implementing the proposed identification-based closed-loop system to the cell culture experiments. To conclude, we believe that the presented method can be further extended not only to other applications in biological cell studies, but also to different areas, such as microfluidic environmental monitoring and chemical engineering.

ACKNOWLEDGMENT

The authors would like to thank Professor Matti Vilkko for helping with a system identification process, and Doctor Terho Jussila for helpful discussions related to control issues.

REFERENCES

[1] C. Yi, C. W. Li, S. Ji, and M. Yang, "Microfluidics technology for manipulation and analysis of biological cells," *Anal. Chim. Acta*, vol. 560, no. 1–2, pp. 1–23, Feb. 2006.

[2] I.-F. Yu, Y.-H. Yu, L.-Y. Chen, S.-K. Fan, H.-Y. E. Chou, and J.-T. Yang, "A portable microfluidic device for rapid diagnosis of cancer metastatic potential with programmable modules of temperature and CO2," *Lab Chip*, vol. 14, no. 18, pp. 3621–3628, 2014.

[3] E. Seker, J. H. Sung, M. L. Shuler and M. L. Yarmush, "Solving Medical Problems with BioMEMS," *IEEE Pulse*, vol. 2, no. 6, pp. 51-59, Nov.-Dec. 2011.

[4] S. Halldorsson, E. Lucumi, R. Gómez-Sjöberg, and R. M. T. Fleming, "Advantages and challenges of microfluidic cell culture in polydimethylsiloxane devices," *Biosens. Bioelectron.*, vol. 63, pp. 218–231, Jan. 2015.

[5] M. Mehling and T. Savas, "Microfluidic cell culture," *Curr. Opin. Biotechnol.*, vol. 25, pp. 95–102, Feb. 2014.

[6] R. Que and R. Zhu, "A two-dimensional flow sensor with integrated micro thermal sensing elements and a back propagation neural network," *Sensors*, vol. 14, no. 1, pp. 564–74, Jan. 2014.

[7] S. Petronis, M. Stangegaard, C. B. Christensen, and M. Dufva, "Transparent polymeric cell culture chip with integrated temperature control and uniform media perfusion," *Biotechniques*, vol. 40, no. 3, pp. 368–376, Mar. 2006.

[8] F. Abeille, F. Mittler, P. Obeid, M. Huet, F. Kermarrec, M. E. Dolega, F. Navarro, P. Pouteau, B. Icard, X. Gidrol, V. Agache, and N. Picollet-D'hahan, "Continuous microcarrier-based cell culture in a benchtop microfluidic bioreactor," *Lab Chip*, vol. 14, no. 18, pp. 3510-3518, Sep. 2014.

[9] D. Saalfrank, A. K. Konduri, S. Latifi, R. Habibey, A. Golabchi, A. V. Martiniuc, A. Knoll, S. Ingebrandt, and A. Blau, "Incubator-independent cell-culture perfusion platform for continuous long-term microelectrode array electrophysiology and time-lapse imaging," *R. Soc. Open Sci.*, vol. 2, no. 6, pp. 150031, Jun. 2015.

[10] R. Habibey, A. Golabchi, S. Latifi, F. Difato, and A. Blau, "A microchannel device tailored to laser axotomy and long-term microelectrode array electrophysiology of functional regeneration," *Lab Chip*, vol. 15, no. 24, pp. 4578–4590, Dec. 2015.

[11] J. M. Jang, J. Lee, H. Kim, N. L. Jeon, and W. Jung, "One-photon and two-photon stimulation of neurons in a microfluidic culture system," *Lab Chip*, vol. 16, no. 9, pp. 1684–1690, Apr. 2016.

[12] J. Vukasinovic, D. K. Cullen, M. C. LaPlaca, and A. Glezer, "A microperfused incubator for tissue mimetic 3D cultures," *Biomed. Microdevices*, vol. 11, no. 6, pp. 1155–1165, Dec. 2009.

[13] E. Biffi, G. Regalia, D. Ghezzi, R. De Ceglia, A. Menegon, G. Ferrigno, G. B. Fiore, and A. Pedrocchi, "A novel environmental chamber for neuronal network multisite recordings," *Biotechnol. Bioeng.*, vol. 109, no. 10, pp. 2553–2566, Oct. 2012.

[14] J.-L. Lin, M. -H. Wu, C.-Y. Kuo, K.-D. Lee, and Y.-L. Shen, "Application of indium tin oxide (ITO)-based microheater chip with uniform thermal distribution for perfusion cell culture outside a cell incubator," *Biomed. Microdevices*, vol. 12, no. 3, pp. 389–398, Jun. 2010.

[15] G. Regalia, E. Biffi, S. Achilli, G. Ferrigno, A. Menegon, and A. Pedrocchi, "Development of a bench-top device for parallel climate-controlled recordings of neuronal cultures activity with microelectrode arrays," *Biotechnol. Bioeng.*, vol. 113, no. 2, pp. 403–413, Feb. 2016.

[16] K. I.-K. Wang, Z. Salcic, J. Yeh, J. Akagi, F. Zhu, C. J. Hall, K. E. Crosier, P. S. Crosier, and D. Wlodkowic, "Toward embedded laboratory automation for smart Lab-on-a-Chip embryo arrays," *Biosens. Bioelectron.*, vol. 48, pp. 188–196, Oct. 2013.

[17] R. Reig, M. Mattia, A. Compte, C. Belmonte, and M. V Sanchez-Vives, "Temperature modulation of slow and fast cortical rhythms," *J. Neurophysiol.*, vol. 103, no. 3, pp. 1253–1261, Mar. 2010.

[18] T. Glawdel, Z. Almutairi, S. Wang, and C. Ren, "Photobleaching absorbed Rhodamine B to improve temperature measurements in PDMS microchannels," *Lab Chip*, vol. 9, no. 1, pp. 171–174, Jan. 2009.

[19] D. Ross, M. Gaitan, and L. E. Locascio, "Temperature Measurement in Microfluidic Systems Using a Temperature-Dependent Fluorescent Dye," *Anal. Chem.*, vol. 73, no. 17, pp. 4117–4123, Sep. 2001.

[20] E. Laurila, A. Ahola, J. Hyttinen, and K. Aalto-Setälä, "Methods for in vitro functional analysis of iPSC derived cardiomyocytes - Special focus on analyzing the mechanical beating behavior," *Biochim. Biophys. Acta - Mol. Cell Res.*, vol. 1863, no. 7, pp. 1864–1872, 2016.

[21] L. Ljung, "Convergence analysis of parametric identification methods," *IEEE Trans. Automat. Contr.*, vol. 23, no. 5, pp. 770-783, Oct. 1978.

[22] A. Sebastian and D. Wiesmann, "Modeling and experimental identification of silicon microheater dynamics: A systems approach," *J. Microelectromechanical Syst.*, vol. 17, no. 4, pp. 911–920, Aug. 2008.

[23] J. Kreutzer, L. Ylä-Outinen, P. Kärnä, T. Kaarela, J. Mikkonen, H. Skottman, S. Narkilahti, and P. Kallio, "Structured PDMS Chambers for Enhanced Human Neuronal Cell Activity on MEA Platforms," *J. Bionic Eng.*, vol. 9, no. 1, pp. 1–10, Mar. 2012.

[24] Multi Channel Systems MCS GmbH, Germany, "MEA Amplifier for Inverse Microscopes Manual," 2012. [Online]. Available: http://www.multichannelsystems.com/sites/multichannelsystems.com/files/documents/ manuals/MEA1060-Inv_Manual.pdf

[25] Multi Channel Systems MCS GmbH, Germany, "Temperature Controller TC01/02 Manual," 2015. [Online]. Available: http://www.multichannelsystems.com/sites/multichannelsystems.com/files/documents/manuals/TC01- TC02_Manual_RevG.pdf

[26] J. W. Gardner, "Thermoresistor," in *Microsensors: Principles and applications*, 1st ed., New York: Wiley, 1994, p. 94.

[27] D. C. Duffy, J. C. McDonald, O. J. Schueller, and G. M. Whitesides, "Rapid Prototyping of Microfluidic Systems in Poly(dimethylsiloxane)," *Anal. Chem.*, vol. 70, no. 23, pp. 4974–4984, Dec. 1998.

[28] G. Velve-Casquillas, M. Le Berre, M. Piel, and P. T. Tran, "Microfluidic tools for cell biological research," *Nano Today*, vol. 5, no. 1, pp. 28–47, Feb. 2010.

[29] L. Ljung, "System Identification Toolbox User's Guide." MathWorks Inc., USA, p. 904, 2015. [Online]. Available: http://www.mathworks.com/help/pdf_doc/ident/ident.pdf

[30] A.W.M.J. Van Schijndel, "Integrated Heat Air and Moisture Modeling and Simulation," Ph.D. dissertation, Dept. Built. Environment, Eindhoven Univ. of Tech., Eindhoven, The Netherlands, 2007.

[31] J. -Y. Cheng, M. -H. Yen, C. -T. Kuo, and T. -H. Young, "A transparent cell-culture microchamber with a variably controlled concentration gradient generator and flow field rectifier," *Biomicrofluidics*, vol. 2, no. 2, pp. 024105, Jun. 2008.

[32] L. Lin, S.-S. Wang, M.-H. Wu, and C.-C. Oh-Yang, "Development of an integrated microfluidic perfusion cell culture system for real-time microscopic observation of biological cells," *Sensors*, vol. 11, no. 9, pp. 8395–8411, Aug. 2011.

[33] M. Riley, "Instrumentation and Process Control," in *Cell Culture Technology for Pharmaceutical and Cell-Based Therapies*, CRC Press, 2005, pp. 249–297.

[34] H. Witte, M. Stubenrauch, U. Fröber, R. Fischer, D. Voges, and M. Hoffmann, "Integration of 3-D cell cultures in fluidic microsystems for biological screenings," *Eng. Life Sci.*, vol. 11, no. 2, pp. 140–147, Apr. 2011.

[35] G. V. Kaigala, J. Jiang, C. J. Backhouse, and H. J. Marquez, "System design and modeling of a time-varying, nonlinear temperature controller for microfluidics," *IEEE Trans. Control Syst. Technol.*, vol. 18, no. 2, pp. 521–530, Mar. 2010.

Antti-Juhana Mäki received the M.S. degree in automation engineering from Tampere University of Technology (TUT), Tampere, Finland, in 2010. Since 2011, he has been working toward the Ph.D. degree in automation engineering at the Department of Automation Science and Engineering, TUT, under the supervision of Prof. Kallio. Currently, he is working on the development of control system for automated human stem cell environment. His research interests include control engineering, modeling, microfluidics and autonomous systems for cell engineering.

Tomi Ryynänen received his M.Sc. degree in applied physics from University of Jyväskylä in 2000. After a couple of years in optoelectronics and software industry he has been working at Tampere University of Technology since 2005. In addition to doctoral studies he has been responsible for developing the cleanroom laboratories and microfabrication activities at the department of Automation Science and Engineering. His research is focused on microelectrode arrays (MEAs) and other microsensors for cell culturing applications. He has authored or co-authored over 20 international journal or conference papers and one patent application.

Jarmo Verho is working as a research assistant at the Department of Automation Science and Engineering, Tampere University of Technology. He is specialized in low-noise electronics design and embedded systems. His other research interests include sensor networks, radio networks, short range inductive links and capacitive sensing techniques.

Joose Kreutzer received the B.Eng. degree in Electrical and Electronic Engineering from University of Sunderland, Sunderland, England, in 2003 and M.Sc. degree in Electrical Engineering from Tampere University of Technology (TUT), Tampere, Finland, in 2005. In 2001, he joined first time the Department of Automation Science and Engineering, TUT, where he is currently a Research Scientist in the Micro- and Nanosystems Research Group. His research interests include microfabrication, microfluidics, and their applications in biomedical engineering, especially for stem cell based bioengineering.

Jukka Lekkala received the M.Sc. degree in electronics and the D.Sc. (Tech.) degree in biomedical engineering from the Tampere University of Technology (TUT), Tampere, Finland, in 1979 and 1984, respectively. Since 1991, he has been a Docent of bioelectronics at the University of Oulu, Oulu, Finland, and a Docent of biomedical engineering at TUT. Currently, he is a Professor of Automation Technology with the Department of Automation Science and Engineering, TUT. His research activities include sensors, measurement systems, and biosensing.

Pasi J. Kallio (M'03) received his M.S. degree in electrical engineering and D.Tech. degree in automation engineering from Tampere University of Technology (TUT), Tampere, Finland in 1994 and in 2002, respectively. Since 2008, he has been a Professor of Automation Engineering at TUT. He is an author of more than 120 articles, and more than 10 patent applications. His research interests include microrobotics, microfluidics and their automation in cell and tissue engineering, medical diagnostics and soft material testing applications. Prof. Kallio is a member of several societies in IEEE, he was the chair of IEEE Finland Section 2012-2013, and was a recipient of the Finnish Automation Society Award in 2009.